Observation and Quantification of CO2 passive degassing at Sulphur Banks from Kilauea Volcano using thermal Infrared Multispectral Imaging.

Stephane BOUBANGA TOMBET*, Eric GUYOT

Telops Inc., 100-2600 St-Jean-Baptiste Avenue, Québec, QC, Canada G2E 6J5
*(Corresponding author: stephane.boubanga@telops.com)

Abstract - We conducted Thermal Infrared imaging and quantification of CO_2 passive degassing at Sulphur Banks from Kilauea volcano using Telops Midwave Infrared time-resolved multispectral imager. With appropriate spectral filters providing spectral selectivity we estimated the gas transmittance and temperature. Quantitative chemical maps with local CO_2 concentrations of few hundreds of ppm was derived and mass flow rates of few g/s were also estimated. The results show that thermal infrared multispectral imaging provides unique insights for volcanology studies.

Nomenclature (11 pt, 2 columns)

L	radiance, $W \cdot m^{-2} \cdot sr^{-1}$	τ	transmittance
IBR	In-band radiance, $W \cdot m^{-2} \cdot sr^{-1}$	ρ	concentration, ppm
l	path length, m	κ	molar absorptivity, $ppm^{-1} \cdot m^{-1}$
m	mass density, g/m	c	path length concentration, ppm.m
d	pixel size, m	σ_{gas}	gas density, g/m^3.
F	flow rate, g/s	v	mean gas velocity, m/s

1. Introduction

Generally, volcano emissions contain significant proportions of water vapor (H_2O) and carbon dioxide (CO_2), along with variable proportions of toxic/corrosive gases such as sulfur dioxide (SO_2), hydrogen chloride (HCl), hydrogen fluoride (HF), and silicon tetrafluoride (SiF_4) [1]. Among those volcanic gas species, carbon dioxide is the least soluble in basaltic liquids [2]. Additionally, while the emissions of certain volcanic gas species such as SO_2 may be lost totally due to their interactions with groundwater (hydrolysis of SO_2 to aqueous H_2S and sulfate for instance), carbon dioxide is less susceptible to scrubbing by water [3]. The scrubbing and solubility properties of CO_2 underlines the importance of volcanic CO_2 emission rates in the biogeochemical cycle of carbon on planet Earth, as well as its importance in the evaluation of volcanic hazards [4,5]. Measurements and quantification of CO_2 emission rates from volcanoes remain challenging, mainly due to the presence of high background CO_2 in the atmosphere [6]. Additional challenges are related to the unpredictable behavior of volcanos and the life-threatening situations they may create to human lives and scientific instruments. Therefore, remote sensing measurements techniques are highly desirable for the investigation of volcanic gas species emission rates, including CO_2. Among remote sensing techniques, thermal infrared imaging spectroscopy is particularly well-suited for the characterization of volcanic activity, since many volcanic gases including CO_2 and sulfur dioxide (SO_2) are infrared-active molecules. In order to acquire spectral information using thermal infrared cameras, the spectral response of the camera can be tuned using, for instance, an interferometer-based infrared spectrometer (Telops Hyperspectral cameras) or spectral filters (Telops Multispectral camera). In the later case, band-pass (BP), long-pass

https://doi.org/10.25855/SFT2022-056

(LP) and high-pass (HP) spectral filters can readily be added to the camera optical path. Filter wheel systems allow for the storage of a selection of spectral filters readily available for acquisition. Multiple images of the same scene can thus be acquired using different spectral filters, representing a capability set that falls between high-speed broadband imaging and high-spectral resolution hyperspectral imaging. Spectral information is obtained from the response of individual spectral filters, ratios, subtractions and/or combinations of multiple filters. In general, a greater number of spectral bands provide more flexibility for challenging measurement situations.

When investigating volcanic gas emissions, high speed data acquisition ensures a high temporal resolution for the measurement. For this reason, the Telops MS-IR systems are equipped with a fast-rotating motorized filter wheel synchronized with image acquisition (Figure 1). Sequences are calibrated using in-band photon radiance (IBR) format, frame by frame, according to their respective spectral filter dataset. This allows the user to automatically collect frames on each spectral channel without having to handle and/or select filters manually. The Telops MS-IR infrared camera's filter wheel allows storage of up to eight (8) different filters (Figure 1), providing enhanced flexibility over most filter wheel systems on the market. Due to its time-resolved capabilities and its spectral information, the MS system from Telops has proven to be particularly appropriate for gas cloud imaging [7].

In this work, gas detection and quantification measurements were conducted at the Sulphur Banks from Kilauea Volcano using a Telops MS-IR MW camera. All data was collected in in-band radiance format. A physical radiative transfer model was established to describe the contributions from all sources to the observed sensor signal. This radiative transfer model can be solved to obtain gas temperature and concentration at the individual pixel level.

Sulphur Banks is well known for continuous low-level emissions of volcanic gases along with groundwater steam. These gases are rich in carbon dioxide, sulfur dioxide and hydrogen sulfide. Measurements were carried out at a spatial resolution of 4 mm^2/pixel with bandpass spectral filters leading to successfully identification and quantification of carbon dioxide (CO_2) from its distinct spectral features.

2. Experiments

The camera used for this measurement campaign is the MS-IR MW with spectral range covering between 3 to 4.9 μm. The filter configuration (Figure 2) consists of one sapphire window (filter #1) and one neutral density filter OD1 (filter #2) representative of the broadband channels and six spectral filters: BP 4665 nm, BW 240 nm (filter #3), BBP 4358-4534 nm (filter #4), BBP 3725-4245 nm (filter #5), BBP 3575-4125 nm (filter #6), BBP 3440-4075 nm (filter #7) and BBP 2900-3500 nm (filter #8). Acquisitions were carried out at full FPA frame (640×512 pixels) and the integration times were set between 300 and 6300 μs depending on the acquisition channel. Total acquisition frame rate was set to 80 Hz, which gives an effective frame rate of 10 Hz per channel. A MW optical lens of 50 mm was used and the distance between the camera and the target 2 m leading to a spatial resolution of 4 mm^2/pixel. Figure 3 depicts the location of a borehole drilled in 1922 for underground heat measurements at Sulphur Banks. The Telops camera measuring volcanic gas exhausting form the borehole is also shown as well as a typical broadband IR image with the gas plume.

3. Image Processing

A radiative transfer model was established to describe the phenomenology associated with the gas plume detection experiment. For each direction, the infrared scene may be

decomposed into 3 distinct contributions. Starting from the instrument, there are atmospheric layers, the plume released by the volcano, and the background. The first contribution is made of the atmospheric mass between the plume and the IR camera. This air mass is here assumed uniform. Next, the plume is including everything getting out of the volcano that would otherwise not be present in the atmosphere. Finally, the background represents what is behind the plume, referred at the plume level. We assume that the scattering processes are neglectable, the background is therefore fully characterized by the spectral radiance it shines on the plume in the direction of the instrument. The scene may be globally represented as a 2-layer model. Starting with an opaque surface representing the background, 2 semi-transparent layers are added to model the plume and the atmosphere between the plume and the instrument. When required, the model of the plume itself may be made of multiple layers to better represent the plume temperature non-uniformity across its section. Applying recursively the Beer-Lambert-Bouguer's law of spectral radiance being transmitted by the kth homogeneous absorbing layer [8] to all layers, starting from the background up to the atmosphere layer results in:

$$\mathcal{L}_{tot} = [L_{bkg}\tau_{gas} + L_{gas}(1-\tau_{gas})]\tau_{gas} + L_{atm}(1-\tau_{atm}) \quad (1)$$

where explicit dependences upon space and directions have been removed to ease the writing. L corresponds to the radiance and τ corresponds to the transmittance. The background (bkg), the atmosphere (atm), and the gas from the plume (gas) are the main contributors to the total radiance (L_{tot}) measured at sensor level (see Figure 4). For the gas plume, only carbon dioxide was considered in this work due to the configuration of spectral filters available during measurements. We analyzed data in terms of In-band radiance (IBR) which is determined by integrating the measured radiance over a defined spectral range (spectral filters). This process is done during the camera calibration by measuring the output signal while the camera combined with each filter views a blackbody source of a known radiance. During measurements the scene radiance seen though each filter (In-band radiance) is directly therefore directly accessible. By combining the information from all spectral channels, IBR profiles are obtained for each pixel. Optimization of the equation above was carried out on the IBR profile of each pixel in order to estimate the gas plume temperature and its column density. The fit is done by taking the mean square of the difference between the computed radiance ($\mathcal{L}_{tot}$) of Equation 1 and the radiance measured on each pixel by the camera within the 8 spectral filters ($\mathcal{L}_{measured}$) namely In-band radiance profile, $\delta^2 = (\mathcal{L}_{measured} - \mathcal{L}_{tot})^2$. The gas transmittance and thermodynamic temperature on each pixel are obtained by finding the minimum of δ^2 and the gas concentration is then derived from the obtained transmittance. The simulated IBR profiles ($\mathcal{L}_{tot}$) were carried out using the HITRAN spectroscopic database.

4. Results

At Sulphur Banks, volcanic water vapor seeps out of the ground mixed with volcanic gases mainly composed of carbon dioxide, sulfur dioxide and hydrogen Sulphide. A representative MWIR brightness temperature spectrum of a representative gas mixture is depicted in Figure 2. The different spectral filters used during the measurement campaign are also shown for illustration purposes. The strong spectral features of CO_2, seen between 4.15 and 4.5 μm, are associated with the C=O asymmetric stretch vibration. Some weak spectral features associated with water vapor can also be seen around 3.25 and 4.8 μm. Figure 5 shows selected acquisitions of the gas vent recorded through relevant spectral channels. Data from each frame was normalized using the IBR of a blackbody source at 20 °C. The most pronounced thermal contrasts for CO_2 are obtained through filters #4 and #5 since the CO_2 contribution to the signal observed through these filters is relatively high. The thermal contrast observed in

the broadband channel (filter #1) is reduced compared to filters #4 and #5 because the relative contribution to the total signal due to CO_2 emission is smaller in the broadband channel. The thermal contrast observed in filters #3 and #8 are attributed to water vapor. Very small contrasts associated gases exhaust can be seen through the other filters (see filters #7) which can be useful for obtaining information about the background radiance. Such information is necessary for accurate estimation of the gas temperature and concentration using the radiative transfer model discussed above.

4.1. In-band photon radiance profile optimization

A typical IBR profile associated with the volcanic gas emission is shown in Figure 6. Broadband imagery does not allow the user to resolve the chemical nature of targets in the investigated scene due to the lack of spectral information. Comparing the signal obtained in different channels (Fig. 5) with the MS camera in terms of thermal contrast already gives an additional level of information about the chemical nature of the gases seeping out of the borehole. However, thermal contrast would only allow qualitative spectral analysis since the detector response in a single channel is function of many parameters and subject to interfering agents. In order to unambiguously identify and quantify the gases emanating from the borehole, Equation 1 was used to fit the measurement data (See Fig. 6). The IBR profile is computed by integrating the Planck curve equation over the spectral range of each filter. The IBR of a selected target can be estimated for each filter according to its spectral emissivity/transmittance for defined gas concentration and thermal contrast conditions. Selected gas concentration can then be estimated by correlating the estimated IBR profile with measured IBR profiles of individual pixels in a scene. The gas thermodynamic temperature and transmittance are therefore retrieved allowing estimation of gas concentration.

4.2. Gas Quantification

4.2.1. Gas concentration

The column density of CO_2 maps of four different acquisitions are shown on Fig. 7. Quantification was performed by fitting the radiative transfer model (Equation 1) with a non-linear optimization routine in order to estimate the relative contribution of each parameter of the equation to the total measured radiance signal. The gas transmittance $\tau_{gas} = \exp(-\Sigma\, \kappa l \rho)$ in Eq.1 is function of gas concentration ρ (expressed in ppm), path length l (expressed in meters) and the gas molar absorptivity κ. CO_2 gas column density values of up to 35 ppm.m were obtained around the investigated exhaust hole. When the dimensions of the plume are known, the column density path length dependence can be factorized in order to retrieve the gas concentration ρ in ppm. Figure 8 depicts the maximum local CO_2 concentration versus acquisition time at two different locations near the vent hole. The lines labeled line # 1 and line #2 on the top left panel of Fig.7 show the locations where the local concentrations were estimated. The contribution of background CO_2 in the atmosphere was taken into account in τ_{atm} along with the other atmospheric gas species such as N_2O and water vapor. Concentrations of several hundreds of ppm were observed in the vicinity of the exhaust hole, dropping down to few tens of ppm approximately 10 cm away, most likely due to the wind spreading and diluting the gas into the atmosphere.

4.2.2. Velocity Estimation using Optical Flow

A dynamic flow analysis based on a pixel per pixel temporal radiance variation technique was carried out to estimate the gas cloud velocity [9]. The accuracy of this technique strongly depends on the camera acquisition frame rate versus the actual wind dynamics. The high-speed MS Telops camera used in this work allowed gas cloud velocity estimation with about +/- 0.5 m/s error. The mean velocity maps obtained for selected acquisitions are shown in Figure 9. The red arrows correspond to local velocity vectors of different orientations and magnitudes. An example of the estimated gas velocity surrounding the pixel [X, Y] = [344, 222] is also shown in Fig.9 with velocity of [U, V] = [226, 303] pixels/s, where U is the horizontal and V is the vertical velocity. Gas cloud velocities of several m/s were obtained. Wind speed velocity can also be obtained from local meteorological data.

4.2.3. Mass density

From the path length concentration results (Fig.7), we calculate the CO_2 mass density within a specified area of the image using Equation 2:

$$m = \Sigma c \times d \times \sigma_{gas} \qquad (2)$$

where c is the gas path length concentration (ppm.m), d is the pixel size (m), σ_{gas} is the gas density (g/m^3). Total CO_2 mass of 87 mg was obtained within the area of interest shown in white on the top right panel of Fig.7.

4.2.4. Mass Flow Rates

The mass flow rate (flux) in g/s is calculated using the average mass density in a selected area and the mean gas velocity as shown in Equation 3:

$$\boldsymbol{F} = m \times \boldsymbol{v} \qquad (3)$$

where m is the mass density, and $\boldsymbol{v}$ is the mean gas velocity or wind speed. Figure 10 shows the estimated CO_2 mass flow rate obtained for different acquisitions. The estimated values fluctuate significantly from acquisition to acquisition most likely due to changing wind conditions. Good knowledge of wind parameters is essential to improve the precision of the quantification results. Variability and uncertainties on the flow rate estimation may come from the concentration map and linear mass density estimation depending on the precision of the fit of data with Eq.1. Uncertainties may also originate from the gas cloud velocity estimation.

5. Conclusion

Time-resolved multispectral imaging allows efficient investigation of passive or active volcanic degassing. The Telops multispectral imaging system provides spectral information without sacrificing the imaging frame rate required in such situations. IBR profiles drawn from 8 acquisition channels provide good spectral selectivity. The additional information brought by dynamic multispectral imaging over conventional thermal cameras brings new possibilities for infrared signature measurements. Our methodology produces CO_2 column density measurements within the volcano's plume which are used to estimate CO_2 concentration. Quantitative chemical maps with local CO_2 concentrations of hundreds of ppm were derived and corresponding mass flow rates of tens g/s were also estimated. The results show that thermal infrared multispectral imaging can provide unique insights for volcanology studies.

References

[1] Symonds, R. B., W. I. Rose, G. J. S. Bluth, and T. M. Gerlach, Volcanic gas studies: Methods, results, and applications, in Volatiles in Magma, Reviews in Mineralogy, vol. 30, edited by M. R. Carroll and J. R. Holloway, 1-66, Mineralogical Society of America, Washington, D.C., (1994).

[2] Holloway, J. R., and J. G. Blank, Application of experimental results to C-O-H species in natural melts, in Volatiles in Magma, Reviews in Mineralogy, vol. 30, edited by M. R. Carroll and J. R. Holloway, 187-230, Mineralogical Society of America, Washington, D.C., (1994).

[3] Doukas M. P., and T. M. Gerlach, Sulfur dioxide scrubbing during the 1992 eruptions of Crater Peak, Mount Spurr volcano, Alaska, in U.S. Geol. Surv. Bull., 2139, 47-57, (1995).

[4] Berner, R . A., Global CO2 degassing and the carbon cycle: Comment on "Cretaceous ocean crust at DSDP sites 417 and 418: Carbon uptake from weathering vs. loss by magmatic outgassing," Geochim. Cosmochim. Acta, 54, 2889-2890, (1990).

[5] Gerlach, T. M., H. Delgado, K. A. McGee, M.P. Doukas, J. J. Venegas, and L. Cardenas, Application of the LI-COR CO2 analyzer to volcanic plumes: A case study, volcan Popocatepetl, Mexico, June7 and 10, 1995, J. Geophys Res.,102, 8,005-8,019, (1997).

[6] Andres, R. J., and W. I. Rose, Remote sensing spectroscopy of volcanic plumes and clouds, in Monitoring Active Volcanoes, edited by McGuire, B., C. Kilburn, and J. Murray, pp. 301-314, UCL Press Ltd., London, (1995).

[7] Marc-André Gagnon, Karl-Alexandre Jahjah, Frédéric Marcotte, Pierre Tremblay, Vincent Farley and Martin Chamberland. "Time-resolved thermal infrared multispectral imaging of gases and minerals," Proc. of SPIE 9249, (2010)

[8] Hanel R. A., Conrath B. J., Jennings D. E., Samuelson R. E., [Exploration of the Solar System by Infrared Remote Sensing], Cambridge University Press, Cambridge, U.K. (1992).

[9] Horn, B.K.P., Schunck, B.G., Determining Optical Flow, 17, 185-203 (1981).

6. Figures

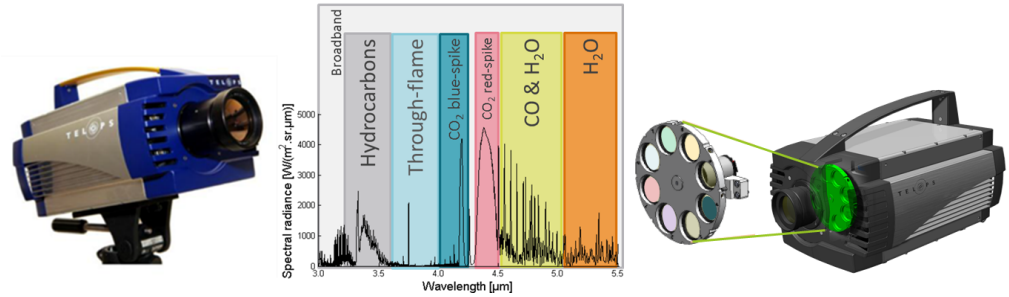

Figure 1: *The MS-IR camera (left) and the filter wheel system (right)*

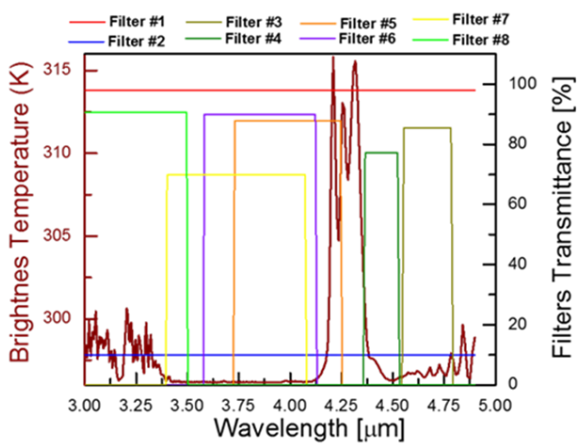

Figure 2 : *MWIR spectrum of gas mixture shown in brightness temperature overlaid on the transmittance of the 8 spectral filters.*

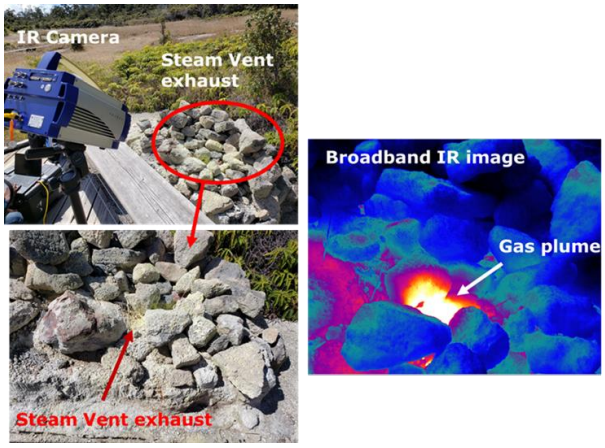

Figure 3 : *Photographs of the gas exhaust hole where measurements were conducted and a typical Broadband IR image of the gas plume.*

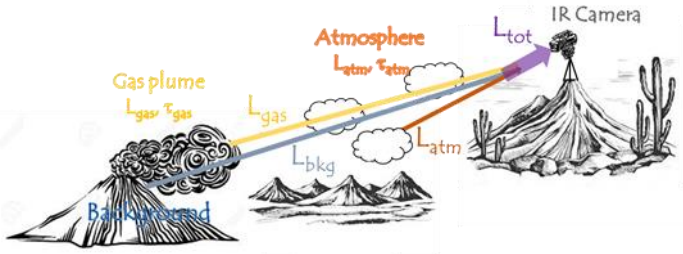

Figure 4: *Illustration of radiative transfer between the volcano and the IR camera.*

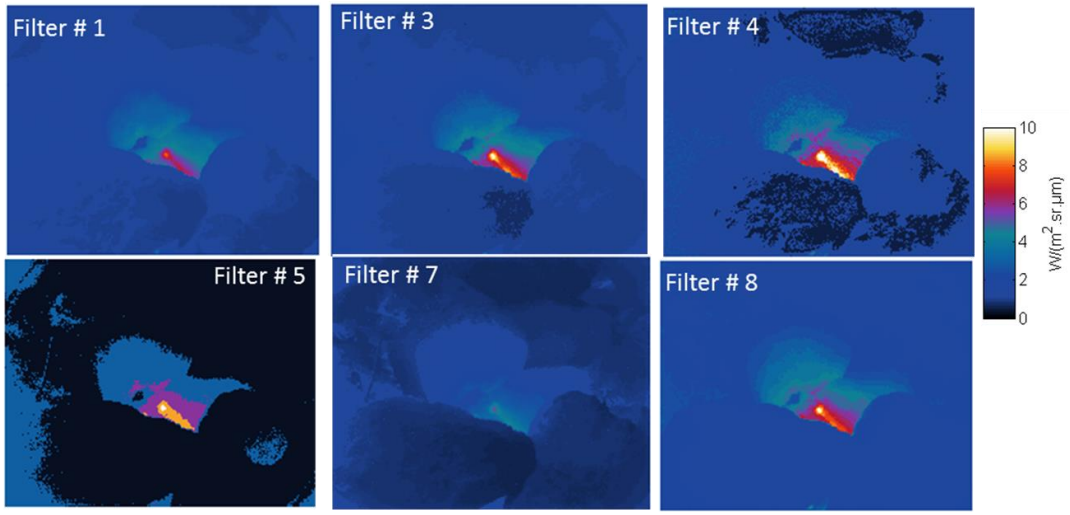

Figure 5: *Normalized responses (blackbody at 20 °C) of selected relevant acquisition channel for multispectral imaging experiment on volcanic gas vent.*

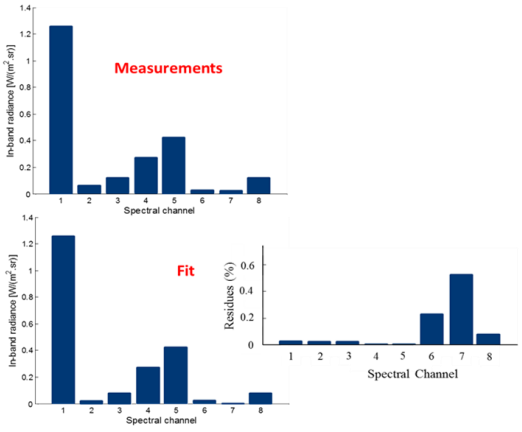

Figure 6 : *Typical measured and Fit In-band radiance (IBR) profiles.*

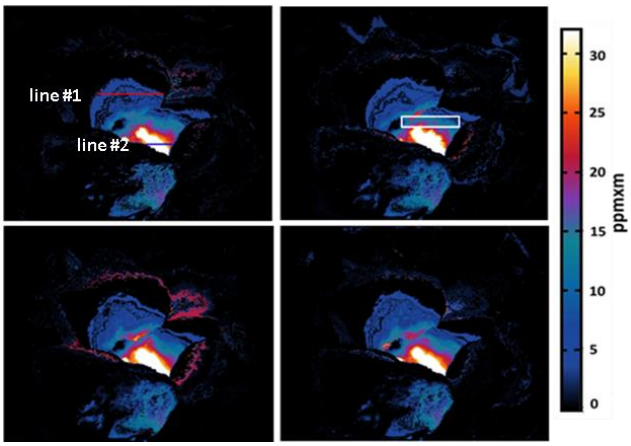

Figure 7 : *CO_2 Column density extracted for measurements using Eq.1.*

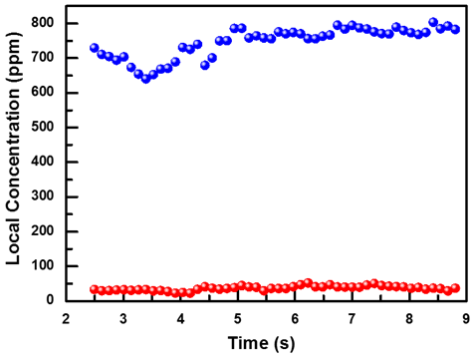

Figure 8 : *CO_2 Local concentration in vicinity of the exhaust hole (bleu dotes) and 10 cm away (red dotes).*

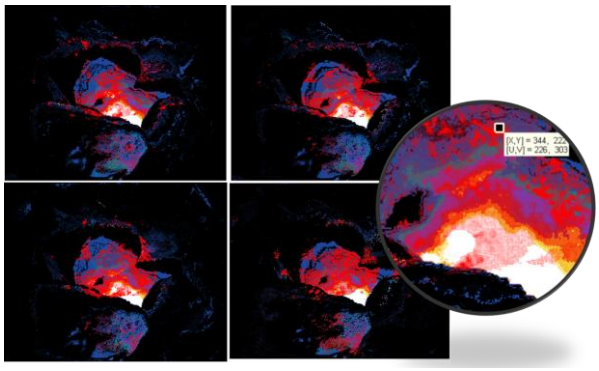

Figure 9 : *Local velocity map obtained after optical flow analysis displayed over the infrared image for clarity purposes.*

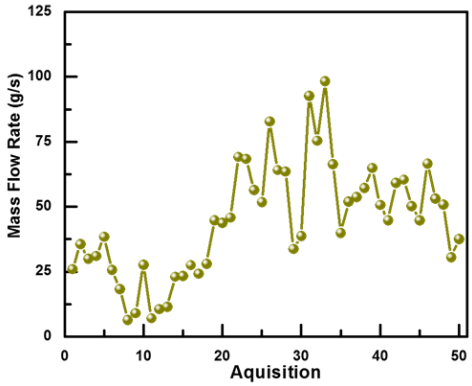

Figure 10: *CO_2 mass flow rate estimates as a function of time.*